Influencing the Morphology and Phase of Calcium Ceramic Nanoparticles Based on the Calcium Alkoxide Precursors' Characteristics

Timothy J. Boyle,* Bernadette A. Hernandez-Sanchez, Christina M. Baros, Luke N. Brewer, and Mark A. Rodriguez

Advanced Materials Laboratory, Sandia National Laboratories, 1001 University Boulevard, SE, Albuquerque, New Mexico 87106

Received January 2, 2007. Revised Manuscript Received February 2, 2007

Select members of a series of structurally characterized calcium aryloxides ($Ca(OAr)_2$) were found to influence the morphologies and phases of the final calcium ceramic nanomaterials produced, independent of the process route investigated. The $Ca(OAr)_2$ were synthesized using an amide alcohol exchange route between $[Ca(\mu\text{-}NR_2)(NR_2)]_2$ ($R = Si(CH_3)_3$) and the appropriate aryl alcohol [H-OAr = H-OC_6H_4(R)-2 where $R = CH(CH_3)_2$ (H-oPP), $C(CH_3)_3$ (H-oBP); H-$OC_6H_3(R)_2$-2,6 where $R = CH_3$ (H-DMP), $CH(CH_3)_2$ (H-DIP), and $C(CH_3)_3$ (H-DBP)] along with triphenyl silanol (H-TPS = $OSi(C_6H_5)_3$], in toluene (tol) or tetrahydrofuran (THF). The resulting products were isolated as $H^+[(\mu_3\text{-}O)Ca_2(\mu\text{-}oPP)_2(oPP)(THF)_3]_2\cdot THF]^-$ (**1**), $Ca(oBP)_2(THF)_4$ (**2**), $H^+[(\mu_3\text{-}O)Ca_2(\mu\text{-}DMP)_2(DMP)(THF)_3]_2^-$ (**3**), $\{2[Ca(DIP)_2(THF)_3]\cdot Ca(DIP)_2(THF)_4\}\cdot THF$ (**4a**), $[Ca(\mu\text{-}DIP)(DIP)(THF)_2]_2$ (**4b**), $Ca(DBP)_2(THF)_3$ (**5**), $[Ca(\mu\text{-}DBP)(DBP)]_2$ (**6**), and $Ca(TPS)_2(THF)_4$ (**7**). The coordination of the Ca atoms ranged from trigonal planar to octahedral, forming mono-, di-, and tetranuclear species based on the steric bulk of the ligand and coordination of Lewis basic THF. Solution NMR indicated that these compounds retain their structure in solution, except for **5**, which was found to be disrupted to form a monomer. Vaterite or portlandite nanomaterials were isolated from **3** or **4a**, respectively, independent of the processing route (solvothermal or solution precipitation). The morphology variations were interpreted based on the "precursor structure argument", and the phase variation was attributed to the "precursor's decomposition pathway". Full details of the synthesis and characterization of **1**−**7** as well as the nanomaterials generated therefrom are discussed.

Introduction

Because the properties of nanocrystals are dictated by both their size and their shape, it is not surprising that the number of reports concerning the production of morphologically varied nanoparticles (i.e., nanodots, -rods, -tetrapods, and -multipods) continues to grow. Typically processing conditions (i.e., temperature, time, concentration, nucleation site, surfactants) are cited as the controlling variable in generating these shape specific nanomaterials. Often overlooked, however, is the contribution that the structure of the precursor makes to the final morphology adopted. We have demonstrated this structure−morphology connection for such varied systems as Ge^0 metal,[1,2] CdE (E = S, Se, Te) semiconductors,[3] and ZnO ceramic[4] nanomaterials. As an explanation for the observed phenomena, we presented the "precursor structure argument" (PSA) where the precursor constructs act as the basic building block, directing the final morphology formed.[1−4] As improvements in the physical properties (size and morphology) of nanoparticles continue to be disseminated, little information concerning synthetic control over the crystalline phase of nanomaterials has been proffered.

Controlling the phase is critical for a number of material systems such as the high dielectric constant optoelectroceramic perovskites, which would include the alkaline earth titanate ceramics, A^ETiO_3 (A^E = Ca, Sr, and Ba). We have recently reported on the utility of a single-source double alkoxide precursor that can be used to produce perovskite nanomaterials of A^ETiO_3.[5] This success led us to investigate the utility of the single cation congeners' nanoceramic properties with an emphasis on calcium alkoxides ($Ca(OR)_2$) due to calcium ceramic materials (CaO_x) widespread use in such diverse applications as ROMP catalyst,[6,7] medical applications,[8,9] and phase critical optoelectronic ceramic materials.[5] In addition, a recent report details the utility of

* Author to whom correspondences should be sent: phone (505)272-7625; fax (505)272-7336; e-mail tjboyle@Sandia.gov.

(1) Gerung, H.; Boyle, T. J.; Tribby, L. J.; Bunge, S. D.; Brinker, C. J.; Han, S. M. *J. Am. Chem. Soc.* **2006**, *128*, 5244.
(2) Gerung, H.; Bunge, S. D.; Boyle, T. J.; Brinker, C. J.; Han, S. M. *Chem. Commun.* **2005**, 1914.
(3) Boyle, T. J.; Bunge, S. D.; Alam, T. M.; Holland, G. P.; Headley, T. J.; Avilucea, G. *Inorg. Chem.* **2005**, *44*, 1309.
(4) Boyle, T. J.; Bunge, S. D.; Andrews, N. L.; Matzen, L. E.; Sieg, K.; Rodriguez, M. A.; Headley, T. J. *Chem. Mater.* **2004**, *16*, 3279.
(5) Hernandez-Sanchez, B. A.; Boyle, T. J.; Baros, C. M.; Brewer, L. N.; Headley, T. J.; Tallant, D. R.; Rodriguez, M. A.; Tuttle, B. A. *Chem. Mater.* **2007**, in press.
(6) Zhong, Z. Y.; Schneiderbauer, S.; Dijkstra, P. J.; Westerhausen, M.; Feijen, J. *J. Polym. Environ.* **2001**, *9*, 31.
(7) Zhong, Z. Y.; Dijkstra, P. J.; Birg, C.; Westerhausen, M.; Feijen, J. *Macromolecules* **2001**, *34*, 3863.
(8) Zakharov, N. A.; Polunina, I. A.; Polunin, K. E.; Rakitina, N. M.; Kochetkova, E. I.; Sokolova, N. P.; Kalinnikov, V. T. *Inorg. Mater.* **2004**, *40*, 735.
(9) Green, D. D.; Kannangara, G. S. K.; Milev, A.; Ben-Nissan, B. *Key Eng. Mater.* **2002**, *218-2*, 79.

10.1021/cm0700091 CCC: $37.00
Published on Web 03/21/2007

specific phases of the CaO_x nanomaterials for artwork preservation efforts.[10]

Previously, we have demonstrated the outstanding efficacy of metal alkoxides ($M(OR)_x$) as precursors to complex ceramic materials.[1−5,11−15] To optimize the properties of the desired CaO_x nanomaterials, a systematically varied, well-characterized, structurally varied series of $Ca(OR)_2$ precursors is required. It is therefore surprising that only a handful have been structurally characterized,[16−24] including $Ca_9(OEtOMe)_{18}(H\text{-}OEtOMe)_2$,[17] $[Ca(OPr^n(Bu^t\text{-}2)(OPr^i\text{-}1,3)_2)_2]_2$,[20] $Ca(DMP)_2(DME)_2$ where DMP = dimethoxypropane and DME = dimethoxyethane,[21] $Ca(TBP)_2(THF)_3$ where TBP = 2,4,6-tributyl phenoxide and THF = tetrahydrofuran,[22] $Ca(OC(C_6H_5)_3)_2(THF)_4$,[22] $Ca(DBP\text{-}Me)_2(OTHF)_3$ where DBP = 4-methyl-2,6-dibutylphenoxide and OTHF = tetrahydrofurfuryloxide,[23] $Ca(DBP\text{-}Me)_2THF_3$,[24] $Ca_6(\mu_3\text{-}O)_2(OEt)_8(H\text{-}OEt)_{12}$,[18,19] and recently $[Ca_2(OMes)(\mu\text{-}OMes)_2(\mu_3\text{-}OH)(solv)_x]_2{\cdot}solv$ (solv (x; ·) = THF (3; 3) and ethylene diamine (2; 2 toluene)).[25]

As a result of this void, the synthesis of a series of calcium aryloxides ($Ca(OAr)_2$) was undertaken using an amide alcohol exchange route (eq 1) between calcium amide ($[Ca(\mu\text{-}NR_2)(NR_2)]_2$ or $[Ca(NR_2)_2]_2$ where R = $Si(CH_3)_3$)[26,27] and the appropriate arylalcohol (H-OAr = $H\text{-}OC_6H_4(R)$-2 where R = $CH(CH_3)_2$ (H-oPP), $C(CH_3)_3$ (H-oBP); $H\text{-}OC_6H_3(R)_2$-2,6 where R = CH_3 (H-DMP), $CH(CH_3)_2$ (H-DIP), and $C(CH_3)_3$ (H-DBP) along with H-TPS (H-TPS = $OSi(C_6H_5)_3$). The products isolated were identified by single-crystal X-ray diffraction (XRD) as $H^+[(\mu_3\text{-}O)Ca_2(\mu\text{-}oPP)_2(oPP)(THF)_3]_2{\cdot}THF]^-$ (**1**), $Ca(oBP)_2(THF)_4$ (**2**), $H^+[(\mu_3\text{-}O)Ca_2(\mu\text{-}DMP)_2(DMP)(THF)_3]_2^-$ (**3**), $\{2[Ca(DIP)_2(THF)_3]{\cdot}Ca(DIP)_2(THF)_4\}{\cdot}THF$ (**4a**) and $[Ca(\mu\text{-}DIP)(DIP)(THF)_2]_2$ (**4b**), $Ca(DBP)_2(THF)_3$ (**5**), and $[Ca(\mu\text{-}DBP)(DBP)]_2$ (**6**), in toluene (tol) or THF. In addition, we investigated the triphenyl silanol (H-TPS = $OSi(C_6H_5)_3$) derivative, eq 1, which was identified as $Ca(TPS)_2(THF)_4$ (**7**).

$$[Ca(NR_2)_2]_2 + 4H\text{-}OR \rightarrow 2Ca(OR)_2 + 4H\text{-}NR_2 \quad (H\text{-}OR = H\text{-}OAr \text{ or } H\text{-}TPS) \tag{1}$$

From these newly synthesized $Ca(OAr)_2$, structurally representative precursors (**3** and **4a**) were selected to generate CaO_x nanomaterials. Not surprisingly, the structural variability of these compounds lent control over the final CaO_x morphology based on the PSA,[1−5] but unexpectedly, for the first time control over the crystalline phase of the nanomaterials was observed based on the precursor's decomposition pathway (PDP). This paper details the synthesis and characterization of these compounds along with the initial attempts to generate nanomaterials from representative members of this series of $Ca(OAr)_2$ precursors.

Experimental Section

All compounds described below were handled with rigorous exclusion of air and water using standard Schlenk line and glovebox techniques. All analytical data were collected on dried crystalline samples. Fourier transform infrared (FT-IR) data were obtained on a Bruker Vector 22 MIR spectrometer using KBr pellets under an atmosphere of flowing nitrogen. Thermogravimetric analysis/differential thermal analysis (TGA/DTA) experiments were performed on a Polymer Laboratories STA 1500 instrument under an atmosphere of flowing nitrogen up to 650 °C at a ramp rate of 5 °C/min. Elemental analyses were performed on a Perkin-Elmer 2400 CHN-S/O elemental analyzer. MicroXRD analysis was performed using a Bruker D8 diffractometer with a 1 mm collimator and incident beam Goebel mirror. Scans are typically collected from 5 to 60° 2θ at 0.04° steps at 2 min per step using Cu Kα radiation at 40 kV and 40 mA. All NMR samples were handled and stored under an argon atmosphere and redissolved in THF-d_8 or tol-d_8 at saturated solution concentrations. All solution spectra were obtained on a Bruker DRX400 spectrometer at 399.87 and 100.54 MHz for ^1H and ^{13}C experiments, respectively. A 5 mm broadband probe was used for all experiments. ^1H NMR spectra were obtained using a direct single pulse excitation, with a 10 s recycle delay and eight scan average. The $^{13}C\{^1H\}$ NMR spectra were obtained using a WALTZ-16 composite pulse ^1H decoupling, a 5 s recycle delay, and a $\pi/4$ pulse excitation.

All solvents were used as received (from Aldrich) in SureSeal bottles and handled only under an inert atmosphere of argon. The following compounds were stored under argon upon receipt (Aldrich) and used without further purification: H-oPP, H-oBP, H-DMP, H-DBP, H-TPS, CaI_2, and KNR_2 where R = $Si(CH_3)_3$. $[Ca(NR_2)_2]_2$ was synthesized according to literature reports using CaI_2 and 2 equiv of KNR_2.[26,27]

General Synthesis. As a result of the similarity of the syntheses of **1**−**7** a general preparatory route is presented below with specific details supplied for each of the individual reactions. Under an argon atmosphere in a glovebox, the appropriate H-OAr was slowly added to a stirring solution of $[Ca(NR_2)_2]_2$. After 12 h, the reaction had turned from a pale yellow color to specific colors (listed below) depending on the H-OAr used. No precipitates were observed for any of the HOAr investigated except DBP, which rapidly dissolved upon heating. The reaction mixtures were initially concentrated by rotary evaporation and then allowed to slowly evaporate, yielding X-ray quality crystals. All analyses used dried, crystalline material.

(10) Baglioni, P.; Giorgi, R. *Soft Mater.* **2006**, *2*, 293.
(11) Boyle, T. J.; Bunge, S. D.; Clem, P. G.; Richardson, J.; Dawley, J. T.; Ottley, L. A. M.; Rodriguez, M. A.; Tuttle, B. A.; Avilucea, G.; Tissot, R. G. *Inorg. Chem.* **2005**, *44*, 1588.
(12) Boyle, T. J.; Pedrotty, D. M.; Alam, T. M.; Vick, S. C.; Rodriguez, M. A. *Inorg. Chem.* **2000**, *39*, 5133.
(13) Boyle, T. J.; Schwartz, R. W. *Comments Inorg. Chem.* **1994**, *16*, 243.
(14) Boyle, T. J.; Tyner, R. P.; Alam, T. M.; Scott, B. L.; Ziller, J. W.; Potter, B. G. *J. Am. Chem. Soc.* **1999**, *121*, 12104.
(15) Bunge, S. D.; Boyle, T. J.; Pratt, H. D.; Alam, T. M.; Rodriguez, M. A. *Inorg. Chem.* **2004**, *43*, 6035.
(16) *Conquest*, Version 1.8; Cambridge Crystallographic Data Centre (support@ccdc.cam.ac.uk or www.ccdc.cam.ac.uk, 2004; August 2006 update).
(17) Goel, S. C.; Matchett, M. A.; Chiang, M. Y.; Buhro, W. E. *J. Am. Chem. Soc.* **1991**, *113*, 1844.
(18) Turova, N. Y.; Turevskaya, E. P.; Kessler, B. G.; Yanovsky, A. I.; Struchkov, Y. T. *Chem. Commun.* **1993**, 21.
(19) Yanovsky, A. I.; Turova, N. Y.; Turevskaya, E. P.; Kessler, V. G.; Struchkov, Y. T. *Zh. Neorg. Khim. (Russ. J. Inorg. Chem.)* **1993**, *38*, 779.
(20) Hermann, W. A.; Huber, N. W.; Priermeir, T. *Angew. Chem., Int. Ed. Engl.* **1994**, *33*, 105.
(21) Evans, W. J.; McClelland, W. G.; Greci, M. A.; Ziller, J. W. *Eur. J. Solid State Inorg. Chem.* **1996**, *33*, 145.
(22) Dunne, J. P.; Tacke, M.; Selinka, C.; Stalke, D. *Eur. J. Inorg. Chem.* **2003**, 1416.
(23) Hitchcock, P. B.; Lappert, M. F.; Lawless, G. A.; Royo, B. *Chem. Commun.* **1990**, 1141.
(24) Tesh, K. F.; Hanusa, T. P.; Huffman, J. C.; Huffman, C. J. *Inorg. Chem.* **1992**, *31*, 5572.
(25) Teng, W.; Guino-o, M.; Hitzbleck, J.; Englich, U.; Ruhlandt-Senge, K. *Inorg. Chem.* **2006**, *45*, 9531−9539.
(26) Westerhausen, M.; Schwarz, W. *Z. Anorg. Allg. Chem.* **1991**, *604*, 127.
(27) Tesh, K. F.; Burkey, D. J.; Hanusa, T. P. *J. Am. Chem. Soc.* **1994**, *116*, 2409.

$H^+[(\mu_3\text{-}O)Ca_2(\mu\text{-}oPP)_2(oPP)(THF)_3]_2\cdot THF]^-$ (1). $[Ca(NR_2)_2]_2$ (0.50 g, 0.70 mmol), H-oPP (0.47 g, 3.5 mmol), and THF (∼5 mL) were used to form a clear yellow solution. Yield: 0.34 g (65%). FT-IR (KBr, cm^{-1}): 3059 (s), 2871 (m), 1599 (w), 1442 (s), 1381 (m), 1357 (s), 1110 (s), 892 (m), 762 (m), 722 (m), 706 (s), 650 (w), 116 (m). ^1H NMR (399.9 MHz, THF-d_8): δ 6.70 (1.5H, bs, $OC_6H_4(CHMe_2)$, 6.51 (1.0H, bs, $OC_6H_4(CHMe_2)$, 1.76−1.71 (2.8H, m, $OC_6H_4(CHMe_2)$, J_{H-H} = 1.20 Hz), 1.08 (6.2H, d, $OC_6H_4(CHMe_2)$, J_{H-H} = 3.60 Hz). $^{13}C\{^1H\}$ (100.5 MHz, THF-d_8): δ 129.7, 128.9, 126.7, 126.0, 125.7 ($OC_6H_4(CHMe_2)$), 15.7, 14.4 ($OC_6H_4(CHMe_2)$). Elem anal. Calcd for $C_{82}H_{122}Ca_4O_{15}$: C, 65.30%; H, 8.15%. Found: C, 65.08%; H, 7.94%.

$Ca(oBP)_2(THF)_4$ (2). $[Ca(NR_2)_2]_2$ (0.53 g, 0.74 mmol), H-oBP (0.55 g, 3.7 mmol), and THF (∼5 mL) were used to form a clear yellow solution. Yield: 0.31 g (34%). FT-IR (KBr, cm^{-1}): 3055 (s), 2873 (m), 2359 (w), 1590 (m), 1561 (m), 1541 (w), 1458 (m), 1358 (m), 1200 (m), 1126 (m), 1085 (m), 1051 (m), 927 (w), 818 (s) 682 (w), 591 (w), 558 (w), 507 (w), 418 (w). ^1H NMR (399.9 MHz, THF-d_8): δ 8.23 (1.0H, bs, $OC_6H_4(CMe_3)$), 7.99 (1.0H, bs, $OC_6H_4(CMe_3)$), 7.67 (0.9H, bs, $OC_6H_4(CMe_3)$), 7.46 (0.7H, bs, $OC_6H_4(CMe_3)$), 2.69 (7.2H, s, $OC_6H_4(CMe_3)$). $^{13}C\{^1H\}$ (100.5 MHz, THF-d_8): δ 136.6, 127.4, 126.9, 117.8 ($OC_6H_4(CMe_3)$), 30.0 ($OC_6H_4(CMe_3)$). Elem anal. Calcd for $C_{36}H_{58}CaO_6$: C, 68.97%; H, 9.33%. Found: C, 68.09%. H, 8.62%.

$H^+[(\mu_3\text{-}O)Ca_2(\mu\text{-}DMP)_2(DMP)(THF)_3]_2^-$ (3). $[Ca(NR_2)_2]_2$ (0.50 g, 0.70 mmol), H-DMP (0.42 g, 3.5 mmol), and THF (∼5 mL) were used to form a clear light orange solution. Yield: 0.35 g (75%). FT-IR (KBr, cm^{-1}): 2960 (m), 2362 (w), 1593 (m), 1466 (s), 1234 (s), 1093 (m), 846 (m), 752 (m), 515 (w). ^1H NMR (399.9 MHz, THF-d_8): δ 6.73 (2H, d, $OC_6H_3Me_2$, J_{H-H} = 7.6 Hz), 6.16 (1H, t, $OC6H_3Me_2$ J_{H-H} = 7.2 Hz), 1.08 (28H, $OC_6H_3Me_2$). $^{13}C\{^1H\}$ (100.5 MHz, THF-d_8): δ 128.7, 124.2, 119.5, 114.3 ($OC_6H_3Me_2$), 16.4 ($OC_6H_3Me_2$). Elem anal. Calcd for $C_{72}H_{102}Ca_4O_{14}$: C, 63.97%; H, 7.61%. Found: C, 63.69%. H, 7.23%.

{2[$Ca(DIP)_2(THF)_3$]·$Ca(DIP)_2(THF)_4$}·THF (4a). $[Ca(NR_2)_2]_2$ (1.0 g, 1.4 mmol), H-DIP (1.2 g, 6.9 mmol), and THF (∼5 mL) were used to form a clear green solution. Yield: 0.82 g (46%). FT-IR (KBr, cm^{-1}): 2961 (s), 2869 (m), 1588 (w), 1458 (m), 1431 (s), 1361 (m), 1258 (m), 1120 (m), 1149 (w), 1042 (m), 838 (m), 748 (m). ^1H NMR (399.9 MHz, THF-d_8): δ 6.75 (1.0H, bs, $OC_6H_3(CHMe_2)_2$), 6.30 (0.3H, bs, $OC_6H_3(CHMe_2)_2$), 1.64−1.73(2.6H, m, $OC_6H_3(CHMe_2)_2$), 1.11 (7.1H, m, $OC_6H_3(CHMe_2)_2$). $^{13}C\{^1H\}$ (100.5 MHz, THF-d_8): δ 135.7, 122.6 ($OC_6H_3(CHMe_2)_2$), 14.7 ($OC_6H_3(CHMe_2)_2$). Elem anal. Calcd for $C_{116}H_{190}Ca_3O_{17}$: C, 70.47%; H, 9.69%. Found: C, 70.49%; H, 9.56%.

$[Ca(\mu\text{-}DIP)(DIP)(THF)_2]_2$ (4b). An identical reaction was run, and analytical data were recorded as above for **4a**; however, the reaction was heated prior to crystallization. $[Ca(NR_2)_2]_2$ (1.0 g, 1.4 mmol), H-DIP (1.2 g, 6.9 mmol), and THF (∼20 mL) were used to form a clear green solution. Yield: 0.62 g (41%). FT-IR (KBr, cm^{-1}): 3054 (w), 2958 (s), 2867 (w), 2364 (w), 1587 (m), 1431 (s), 1341 (m), 1260 (m), 1295 (m), 1142 (w), 1102 (m), 1037 (m), 918 (w), 882 (w), 840 (m), 751 (m), 683 (m), 544 (m), 425 (w). Elem anal. Calcd for $C_{64}H_{100}Ca_2O_8$: C, 71.33%; H, 9.35%. Found: C, 70.89%; H, 9.81%.

$Ca(DBP)_2(THF)_3$ (5). $[Ca(NR_2)_2]_2$ (0.52 g, 0.72 mmol), H-DBP (0.74 g, 3.6 mmol), and THF (∼5 mL) were used to form a clear solution. Yield: 0.78 g (72%). FT-IR (KBr, cm^{-1}): 3059 (s), 2911 (m), 1599 (m), 1583 (w), 1442 (m), 1406 (s), 1381 (m), 1357 (s), 886 (m), 706 (s), 650 (m), 1146 (m), 1028 (m), 884 (w), 816 (w). ^1H NMR (399.9 MHz, THF-d_8): δ 6.72 (1.0H, t, $OC_6H_3(CMe_3)_2$, J_{H-H} = 8.0 Hz), 7.1 (2.6H, d, $OC_6H_3(CMe_3)_2$, J_{H-H} = 8.0 Hz), 1.42 (18.8H, s, $OC_6H_3(CMe_3)_2$). $^{13}C\{^1H\}$ (100.5 MHz, THF-d_8): δ 166.9, 129.5, 125.9, 125.2, 1204.5 ($OC_6H_3(CMe_3)_2$), 15.6, 14.3 ($OC_6H_3(CMe_3)_2$). Elem anal. Calcd for $C_{40}H_{66}CaO_5$: C, 72.03%; H, 9.97%. Found: C, 71.73%; H, 10.12%.

$[Ca(\mu\text{-}DBP)(DBP)]_2$ (6). $[Ca(NR_2)_2]_2$ (1.0 g, 1.4 mmol), H-DBP (1.4 g, 6.9 mmol), and tol (∼5 mL) were used to form a clear pink solution. Yield: 0.96 g (76%). FT-IR (KBr, cm^{-1}): 3064 (m), 2962 (m), 2363 (m), 1591 (m), 1560 (m), 1477 (s), 1107 (s), 1037 (m), 1019 (m), 702 (s), 515 (m). ^1H NMR (399.9 MHz tol-d_8): δ 7.46 (1.0H, d, $OC_6H_3(CHMe_3)$, J_{H-H} = 7.6 Hz), 6.85 (0.5H, t, $OC_6H_3(Me_3)$, J_{H-H} = 7.6 Hz), 1.69 (13.0H, s, $OC_6H_3(CHMe_3)$). $^{13}C\{^1H\}$ (100.5 MHz, tol-d_8): δ 136.5, 125.5 ($OC_6H_3(CMe_3)_2$), 34.3, 30.3 ($OC_6H_3(CMe_3)_2$). Elem anal. Calcd for $C_{56}H_{84}Ca_2O_4$: C, 74.61%; H, 9.39%. Found: C, 74.25%; H, 9.45%.

$Ca(TPS)_2(THF)_4$ (7). $[Ca(NR_2)_2]_2$ (0.53 g, 0.74 mmol), H-TPS (0.77 g, 3.7 mmol) and THF (∼5 mL) were used to form a clear solution. Yield: 0.97 g (75%). FT-IR (KBR, cm^{-1}): 3064 (m), 2962 (m), 2363 (m), 1591 (m), 1560 (m), 1561 (s), 1477 (s), 1107 (s), 1037 (m), 1019 (m), 702 (s), 515 (m). ^1H NMR (399.9 MHz THF-d_8): δ 7.62 (s, $OSi(C_6H_5)_3$). $^{13}C\{^1H\}$ (100.5 MHz, THF-d_8): δ 145.7, 136.4, 128.3, 127.6 ($OSi(C_6H_5)_3$). Elem anal. Calcd for $C_{52}H_{62}CaO_6Si_2$: C, 71.03%; H, 7.11%. Found: C, 69.48%; H, 6.89%.

General X-ray Crystal Structure Information.[28] Crystals were mounted onto a thin glass fiber from a pool of Fluorolube and immediately placed under a cold N_2 vapor stream, on a Bruker AXS diffractometer with a SMART 1000 charge-coupled device detector. The radiation used was graphite monochromatized Mo Kα radiation (λ = 0.7107 Å). Lattice determination and data collection were carried out using SMART version 5.054 software. Data reduction was performed using SAINTPLUS version 6.01 software. The data were corrected for absorption using the SADABS program within the SAINT software package.

Structures were solved using direct methods that yielded the heavy atoms, along with a number of the lighter atoms, and subsequent Fourier syntheses yielded the remaining light-atom positions. The hydrogen atoms were fixed in positions of ideal geometry and refined using SHELXS software. The final refinement of each compound included anisotropic thermal parameters for all non-hydrogen atoms. It is of note that crystal structures of metal alkoxides often contain disorder within the atoms of the ligand chain causing higher than normal final correlations.[29−34] All CIF files were checked at http://www.iucr.org/. For **1** and **4a**, it was necessary to model electron density associated with disordered solvent molecules using the Platon program SQUEEZE.[35] An electron count of 71 and 147 e^-/cell with solvent volumes of 292.5 and 873.5 $Å^3$, for **1** and **4a**, respectively, were found. This is in agreement with two and four THF molecules, respectively, per unit cell and one THF per formula unit for both **1** and **4a** structures. The elemental content of the disordered THF molecules was added to the final compositions of **1** and **4a** during the final refinement cycles. Compounds **1** and **3** require a proton to maintain charge neutrality based on an assumed +2 charge for Ca. The H atoms are most

(28) The listed versions of SAINT, SMART, XSHELL, XP in SHELXTL, and SADABS Software (**2000**) were used in the analysis. Bruker Analytical X-Ray Systems, Inc.: Madison, WI.
(29) Bradley, D. C.; Mehrotra, R. C.; Gaur, D. P. *Metal Alkoxides*; Academic Press: New York, 1978.
(30) Bradley, D. C.; Mehrotra, R. C.; Rothwell, I. P.; Singh, A. *Alkoxo and Aryloxo Derivatives of Metals*; Academic Press: New York, 2001; p 704.
(31) Turova, N. Y.; Turevskaya, E. P.; Kessler, V. G.; Yanovskaya, M. I. *The Chemistry of Metal Alkoxide*; Kluwer Academic Publishers: Boston, 2002; p 568.
(32) Caulton, K. G.; Hubert-Pfalzgraf, L. G. *Chem. Rev.* **1990**, *90*, 969.
(33) Chandler, C. D.; Roger, C.; Hampden-Smith, M. J. *Chem. Rev.* **1993**, *93*, 1205.
(34) Hubert-Pfalzgraf, L. G. *New J. Chem.* **1987**, *11*, 663.
(35) Speck, A. L. *Acta. Crystallogr.* **1990**, *A46*, C34.

Table 1. Crystallography Data Collection Parameters for 1−7

compound	**1**	**2**	**3**	**4a**[a]
chemical formula	$C_{82}H_{122}Ca_4O_{15}$	$C_{36}H_{58}CaO_6$	$C_{72}H_{102}Ca_4O_{14}$	$C_{116}H_{190}Ca_3O_{17}$
fw	1508.12	626.90	1351.86	1972.89
temp (K)	203(2)	203(2)	203(2)	203(2)
space group	monoclinic *P*2(1)/*n*	monoclinic *P*2(1)/*c*	monoclinic *P*21/*c*	monoclinic *C*2/*c*
a (Å)	12.5656(8)	9.2990(13)	15.808(2)	40.750(9)
b (Å)	16.0295(10)	14.164(2)	20.981(3)	16.333(4)
c (Å)	21.1322(14)	13.927(2)	22.635(4)	19.166(4)
β (deg)	92.3000(10)	101.170(3)	103.635(3)	111.120(4)
V (Å^3)	4253.0(5)	1799.6(4)	7296(2)	11900(5)
Z	2	2	4	4
D_{calcd} (Mg/m^3)	1.178	1.157	1.231	1.101
μ (Mo Kα; mm^{-1})	0.314	0.215	0.357	0.197
R1[b] (%; all data)	5.19 (6.90)	4.73 (6.34)	8.97 (21.10)	6.86 (13.12)
wR2[c] (%; all data)	14.24 (15.24)	11.20 (12.15)	21.74 (28.60)	15.93 (18.36)

compound	**4b**	**5**	**6**	**7**[a]
chemical formula	$C_{64}H_{100}Ca_2O_8$	$C_{40}H_{66}CaO_5$	$C_{56}H_{84}Ca_2O_4$	$C_{52}H_{62}CaO_6Si_2$
fw	1077.60	667.01	901.39	879.28
temp (K)	203(2)	203(2)	203(2)	203(2)
space group	monoclinic *P*2(1)/*c*	orthorhombic *Pca*2(1)	monoclinic *P*2(1)/*c*	triclinic $P\bar{1}$
a (Å)	19.951(8)	21.576(3)	9.8317(15)	12.2051(15)
b (Å)	14.435(6)	9.7780(13)	14.020(2)	12.8757(16)
c (Å)	21.707(9)	19.013(3)	19.104(3)	15.8624(19)
α (deg)				93.792(2)
β (deg)	99.677(7)		95.659(3)	90.235(2)
γ (deg)				103.998(2)
V (Å^3)	6163(4)	4011.3(9)	2620.6(7)	2412.9(5)
Z	4	4	2	2
D_{calcd} (Mg/m^3)	1.161	1.104	1.142	1.210
μ (Mo Kα; mm^{-1})	0.236	0.195	0.260	0.227
R1[b] (%; all data)	5.78 (9.20)	5.10 (7.92)	4.72 (6.09)	6.20 (10.48)
wR2[c] (%; all data)	11.72 (13.33)	10.10 (11.27)	11.45 (12.41)	13.17 (15.05)

[a] The crystal structure solution has more than one independent molecules in the unit cell. Chemical and formula weights for **4a** represents the three molecules and one THF and for **7** represents only one of the two molecules. [b] $R1 = \sum||F_o| - |F_c||/\sum|F_o| \times 100$. [c] $wR2 = [\sum w(F_o^2 - F_c^2)^2/\sum(w|F_o|^2)^2]^{1/2} \times 100$.

likely associated with an O atom, and an inspection of the angles, distances, and electron maps did not unambiguously reveal the location of the H atoms in **1** or **3**. Additional information concerning the data collection and final structural solutions of **1**−**7** can be found in Supporting Information or by accessing the final CIF files through the Cambridge Crystallographic Data Base. Data collection parameters for **1**−**7** are given in Table 1. For **5**, the noncentrosymmetric setting was chosen because of disorder in THF molecules which breaks the symmetry of the molecule as observed by looking down the *a*, *b*, and *c* axes of the molecule using the XP command MATR of the SHELXTL software package.

Nanoparticle Synthesis. Two routes were used to generate nanoparticle (A) solvothermal and (B) solution precipitation: (A) The solvothermal route involved the dissolution of the desired precursor in benzyl alcohol, sealing the reaction mixture in a Parr acid digestion bomb and heating it to 200 °C for 48 h. After this time, the reaction vessel was allowed to cool to room temperature. For each reaction, a white precipitate was observed. The mother liquor was removed by centrifugation, and the precipitate was washed three times with ethanol (EtOH) and then allowed to dry at room temperature. (B) The solution precipitation route involved the dissolution of the desired precursor in its parent solvent. This room temperature mixture was then injected into a solution of 1-methyl imidazole and water (MeIm/H_2O = 14.5:0.5 mL) at reflux temperatures. After heating for 30 min, the reaction was allowed to cool to room temperature. The precipitate was removed by centrifugation and washed with EtOH.

Independent of the synthesis route, the resulting nanopowders were slurried in toluene followed by placing a drop of the solution onto a holey-carbon copper grid and allowing it to air-dry. Images were obtained using the Phillips CM30 transmission electron microscopy/scanning transmission electron microscopy (TEM/STEM) instrument at 300 keV. Images were collected both in bright field imaging and bright field STEM mode. In addition, the powder was characterized using a PANalytical powder diffractometer using Cu Kα radiation with step size 0.0167°, with a 53.340 s dwelling time. The Ca nanoceramic sample was mounted on a zero background substrate (Si(510)) purchased from the Gem Dugout.

Results and Discussion

As a result of the void in the literature,[16−24] it was necessary to undertake the systematic synthesis of structurally varied $Ca(OR)_2$, using a series of sterically varied, ortho-substituted aryloxides. The OAr ligands were selected because of the previously observed structural variations for other $M(OAr)_x$ systems.[12,15,36] Once fully characterized, two representative $Ca(OAr)_2$ precursors were then used for the production of CaO_x nanomaterials. The synthesis, characterization, and properties of the nanomaterials produced from these novel precursors are discussed below.

Synthesis. The amide alcohol exchange route (eq 1) was favored to synthesize this family of compounds because it reduces the likelihood of halide contamination, and we have previously had a high degree of success using this route for

(36) Boyle, T. J.; Andrews, N. L.; Rodriguez, M. A.; Campana, C.; Yiu, T. *Inorg. Chem.* **2003**, *42*, 5357.

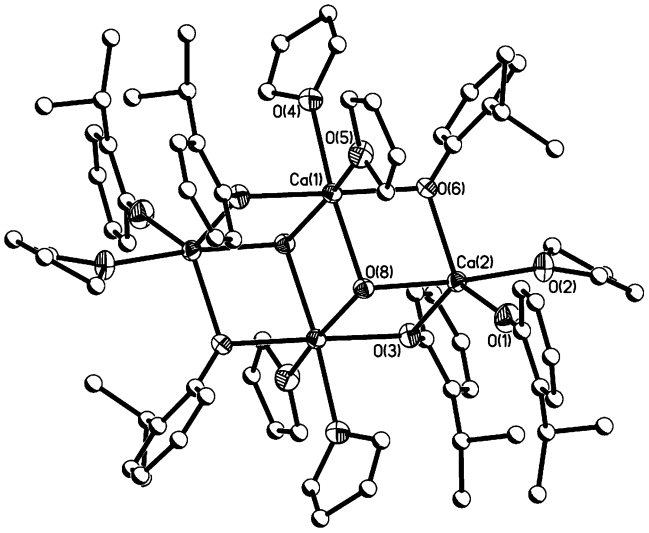

Figure 1. Structure plot of **1**. Thermal ellipsoids of heavy atoms are drawn at the 30% level, and carbon atoms are shown as ball and stick for clarity. Co-crystallized THF is not shown.

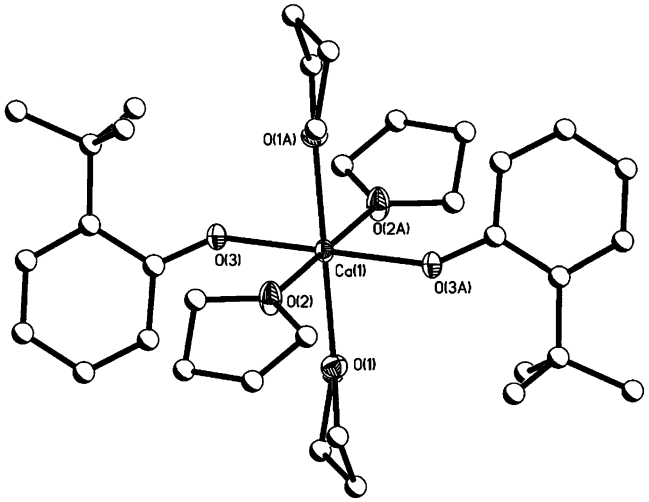

Figure 2. Structure plot of **2**. Thermal ellipsoids of heavy atoms are drawn at the 30% level, and carbon atoms are shown as ball and stick for clarity.

the synthesis of other $M(OR)_x$.[12,15,36] Once isolated, $[Ca(NR_2)_2]_2$[26,27] was reacted with 4 equiv of the appropriate H-OAr in THF at ~25 °C (eq 1) with the exceptions of the DBP adduct (**5**) which was dissolved in toluene. After 12 h of stirring, no precipitates were observed, and the reaction mixtures ranged in color from colorless to yellow to orange to pink to green depending on the ligand. It is of note that the colors observed for these reactions were for the solution and *not* the final white crystalline materials. These colors are therefore not associated with the final products but more likely represent the decomposition of the H-OAr. Crystals were isolated for each sample by slow evaporation of the volatile material in a glovebox under an argon atmosphere. For the following analyses, crystals were dried by rotary evaporation and washed with cold hexanes if necessary, to yield off-white powders that were used without further modification.

On the basis of the observed appropriate bends and stretches for the various OAr ligands, the FT-IR spectra of the bulk crystalline material for **1**−**7** indicated that the amides had been fully exchanged. In general, if very carefully handled, freshly isolated, washed, and dried crystals were used for the elemental analyses, the bulk materials were found to be consistent with the subsequent crystal structures; however, it is of note that during these analyses, a wide variety of compositions were recorded. For solvated $M(OR)_x$ these inconsistencies are often attributed to premature loss of solvent which in this case is THF.[4,11,12,15,36] However, further investigation of the decomposition of these compounds through calcining the precursors in air at 950 °C (conditions similar to the elemental analysis) led to the identification of calcium carbonate as the final material, by powder XRD. This incomplete conversion to CaO may also be used to explain the difficulty we had in obtaining acceptable elemental analyses for the identification of the bulk material.

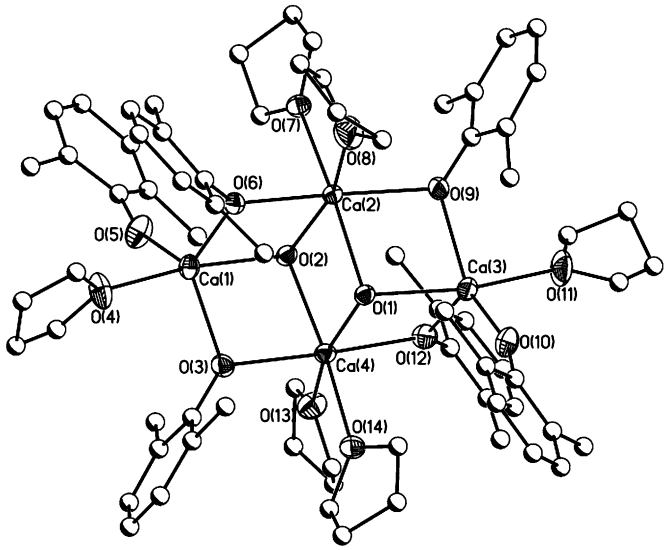

Figure 3. Structure plot of **3**. Thermal ellipsoids of heavy atoms are drawn at the 30% level, and carbon atoms are shown as ball and stick for clarity.

To further characterize these compounds, single-crystal X-ray structures of the products were obtained. The X-ray structures of **1**−**7** are shown in Figures 1−7, respectively. For other $M(OR)_x$ systems, as the steric bulk of the ortho substituent is increased, typically smaller nuclearity species have been identified.[12,15,36] The complexity of the $Ca(OAr)_2$ compounds isolated were found to range from tetra- (**1** and **3**) to di- (**4b** and **6**) to mononuclear (**2**, **4a**, **5**, and **7)** with no correlation readily apparent from the steric bulk of the ortho substitution. The various structural aspects of **1**−**7**, based on nuclearity (smallest to largest), are discussed below and compared to literature compounds when possible.[16−24,37]

Using the monosubstituted oPP ligand, the smallest steric constrained ligand in this set of compounds, a tetrameric oxo species was isolated as **1** (Figure 1). The DMP derivative **3** (Figure 3) also adopts the same structure, which is best described as two face shared cubes with opposite corners missing, or standard M_4O_6 geometry.[38] Two of the four Ca metal centers adopt a trigonal bipyramidal (TBP) geometry using one OR, two μ-OR, and one μ_3-O that bridge to the

(37) Darr, J. A.; Drake, S. R.; Hursthouse, M. B.; Malik, K. M. A. *Inorg. Chem.* **1993**, *32*, 5704.
(38) Boyle, T. J.; Schwartz, R. W.; Doedens, R. J.; Ziller, J. W. *Inorg. Chem.* **1995**, *34*, 1110.

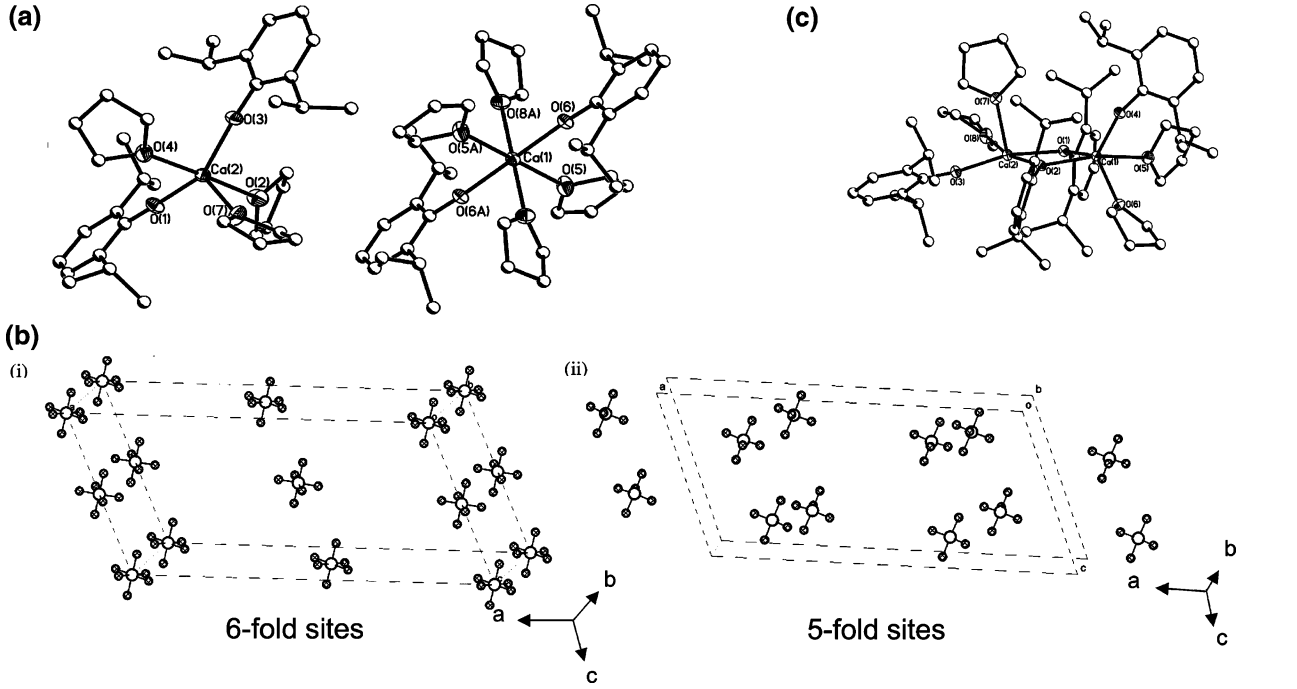

Figure 4. (a) Structure plot of the two geometries observed for **4a.** Thermal ellipsoids of heavy atoms are drawn at the 30% level, and carbon atoms are shown as ball and stick for clarity. **4a** has three independent molecules per unit cell. (b) Illustration of the specific coordination of the packing for **4a**. All C and H atoms have been removed for clarity, showing only the Ca−O coordination for (i) the sixfold and (ii) fivefold packing. (c) Structure plot of **4b**. Thermal ellipsoids of heavy atoms are drawn at the 30% level, and carbon atoms are shown as ball and stick for clarity.

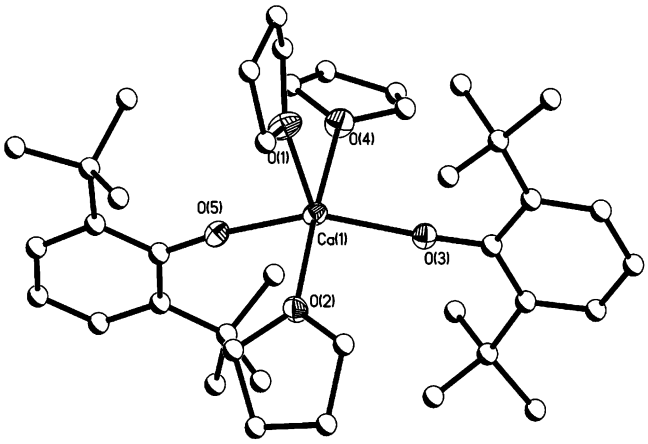

Figure 5. Structure plot of **5**. Thermal ellipsoids of heavy atoms are drawn at the 30% level, and carbon atoms are shown as ball and stick for clarity.

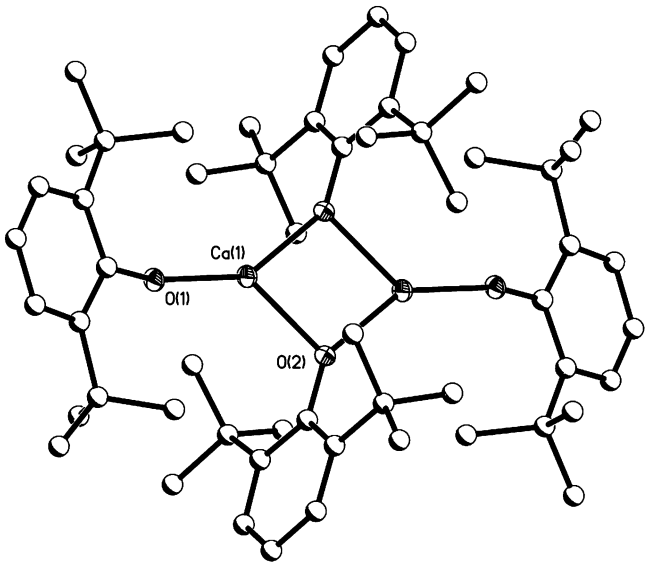

Figure 6. Structure plot of **6**. Thermal ellipsoids of heavy atoms are drawn at the 30% level, and carbon atoms are shown as ball and stick for clarity.

other two octahedrally (Oh) bound Ca metal centers. All of the remaining terminal coordination sites are filled with THF solvent molecules. To maintain charge balance for the Ca^{+2} metal centers, a proton is required. An investigation of the metrical data and the electron map for **1** and **3** did not unequivocally discern the location of the necessary proton. Therefore, the μ_3-O can either be assigned as an oxide with a HOR on the molecule[39] or a hydroxide.[25] The origin of the oxo species is not known as of yet, but because of the non-oxo species isolated for the remainder of the $Ca(OAr)_2$, this must be assumed to be from decomposition of the ligands (as is often claimed for oxo presence in these compounds)[29,30,40] and not due to the synthetic protocols used. A recent report of the 2,4,6-trimethylphenoxide (OMes) derivative which adopts a similar arrangement was reported as the hydroxide species $[Ca_2(OMes)(\mu\text{-}OMes)_2(\mu_3\text{-}OH)(THF)_3]_2$.[25] The H assignment was based on the residual electron density around the μ_3-O atom. Even with the significantly improved structural quality of **1** and **3** in comparison to OMes derivative, we were not able to unambiguously locate the proton. Therefore, we have left **1** and **3** as disordered protonated species.[39] The literature Ca−(μ-O) bond distance range of 2.28−2.39 Å for similarly arranged Ca−O tetrameric compounds[16,41,42] is in agreement

(39) Caulton, K. G.; Chisholm, M. H.; Drake, S. R.; Foltin, K. *J. Chem. Soc., Chem. Commun.* **1990**, 1349−1351.
(40) Turova, N. Y. *Russ. Chem. Rev.* **2004**, *73*, 1041.
(41) Utko, J.; Przybylak, S.; Jerzykiewicz, L. B.; Szafert, S.; Sobata, P. *Chem.−Eur. J.* **2003**, *9*, 181.
(42) Arunasalam, V.-C.; Baxter, I.; Drake, S. R.; Hursthouse, M. B.; Malik, K. M. A.; Otway, D. J. *Inorg. Chem.* **1995**, *34*, 5295.

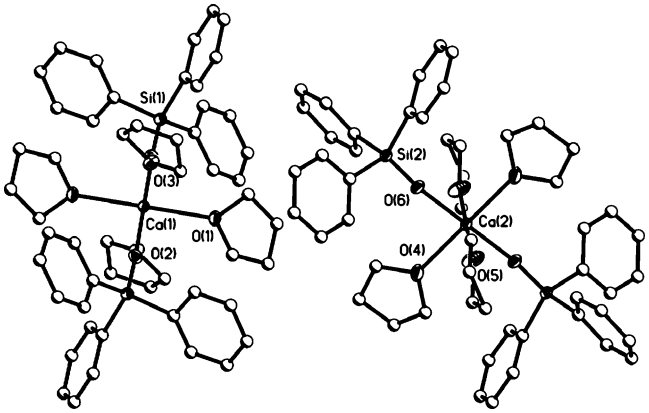

Figure 7. Structure plot of **7**. Thermal ellipsoids of heavy atoms are drawn at the 30% level, and carbon atoms are shown as ball and stick for clarity. **7** has two independent molecules per unit cell (shown).

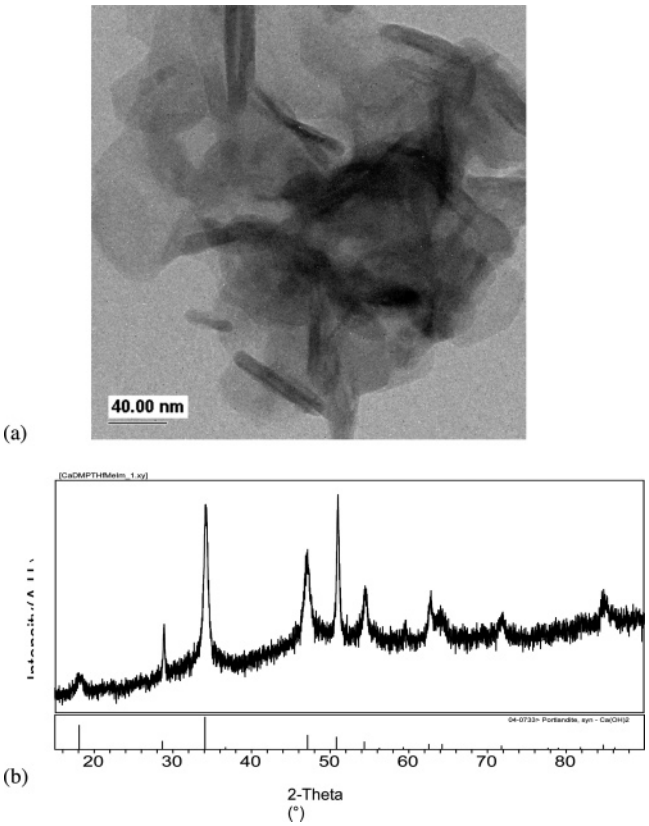

Figure 8. Characterization of portlandite nanomaterials formed from **3** through the solution precipitation route: (a) TEM bright field image and (b) powder XRD pattern.

with the Ca-(μ-O) distances noted for **1** and **3**. The Ca−(μ-O)−Ca angles for the model compounds[16,41,42] range from 101.0 to 109.7°, for (μ-O)−Ca−(μ-O) from 71.0 to 85.1°, and for Ca−(μ_3-O)−Ca from 94.9 to 102.6°, which are in agreement for the angles reported for **1** and **3**. The overall metrical agreement between the literature and these compounds is a little surprising because the model compounds are aminoalkoxy[41] and bidentate alkoxide[42] derivatives. However, the ligand influence of these compounds may be reflected in the (μ_3-O)−Ca−(μ_3-O) angles which range from 80.1 to 99.0°[16,41,42] but does not incorporate the 75.5 to 78.9° range noted for **1** and **3**.

Not surprisingly, as the steric bulk was increased through the introduction of the DBP ligand the nuclearity was

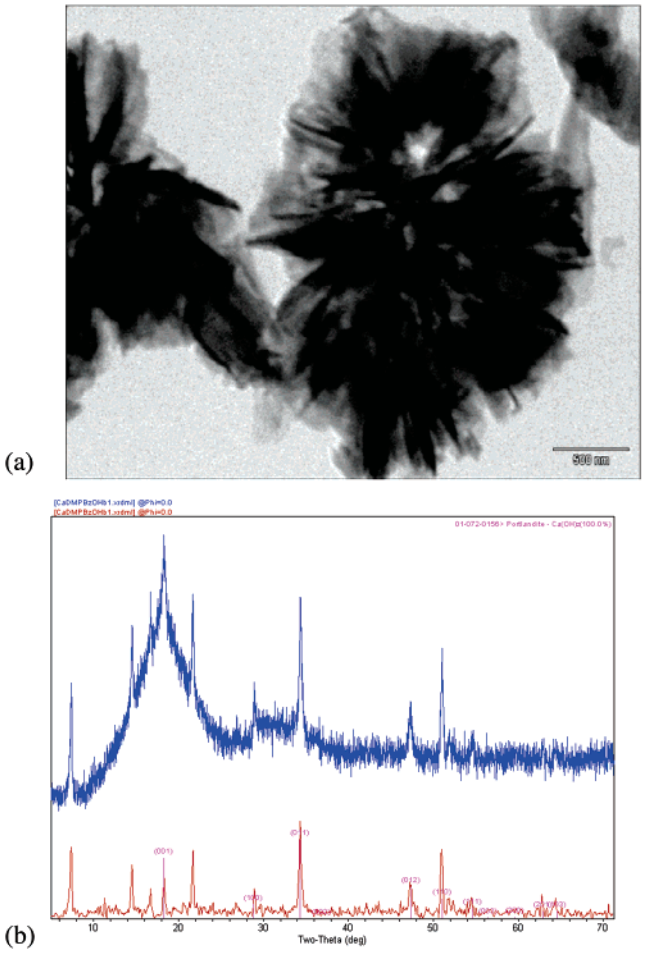

Figure 9. Characterization of portlandite nanomaterials formed from **3** through the solvothermal route: (a) STEM bright field image and (b) powder XRD pattern.

decreased as evidenced through the isolation of the dinculear **6** (Figure 6). For **6**, the Ca metal centers are all trigonal planar with two μ-OR and one terminal OR which is similar to [Ca(μ-DPP)(DPP)]$_2$ where DPP = $OC_6H_3(C_6H_5)_2$-2,6).[43] In addition, the THF/DIP derivative, **4b** (Figure 4c), was also found to adopt a dinuclear structural arrangement, but two solvent molecules of THF are coordinated forming the TBP geometry. The DIP ligand is slightly less sterically demanding than the DBP ligand that allowed for the binding of the THF molecules. The metrical data associated with the literature compound,[41] which has Ca−(μ-O)−Ca angles ranging from 103.9 to 105.3° and (μ-O)−Ca−(μ-O) from 75.25 to 75.32° are not in complete agreement with those of **6** or **4b** (**4b** has angles of 106.1 and 75.0°, and **6** has angles of 101.9 and 78.1°). The variations noted are a reflection of the limited model data set and the binding of Lewis basic solvent molecules. In contrast to the dinuclear **4b**, a more dilute DIP/THF system led to the isolation of monomeric **4a** shown in Figure 4a, wherein additional THF solvent molecules have disrupted the dinuclear species forming a mononuclear solvated compound. As can be observed, compound **4a** possess three molecules in the unit cell with different coordination environments (two TBP and

(43) Deacon, G. B.; Forsyth, C. M.; Junk, P. C. *J. Organomet. Chem.* **2000**, *607*, 112.

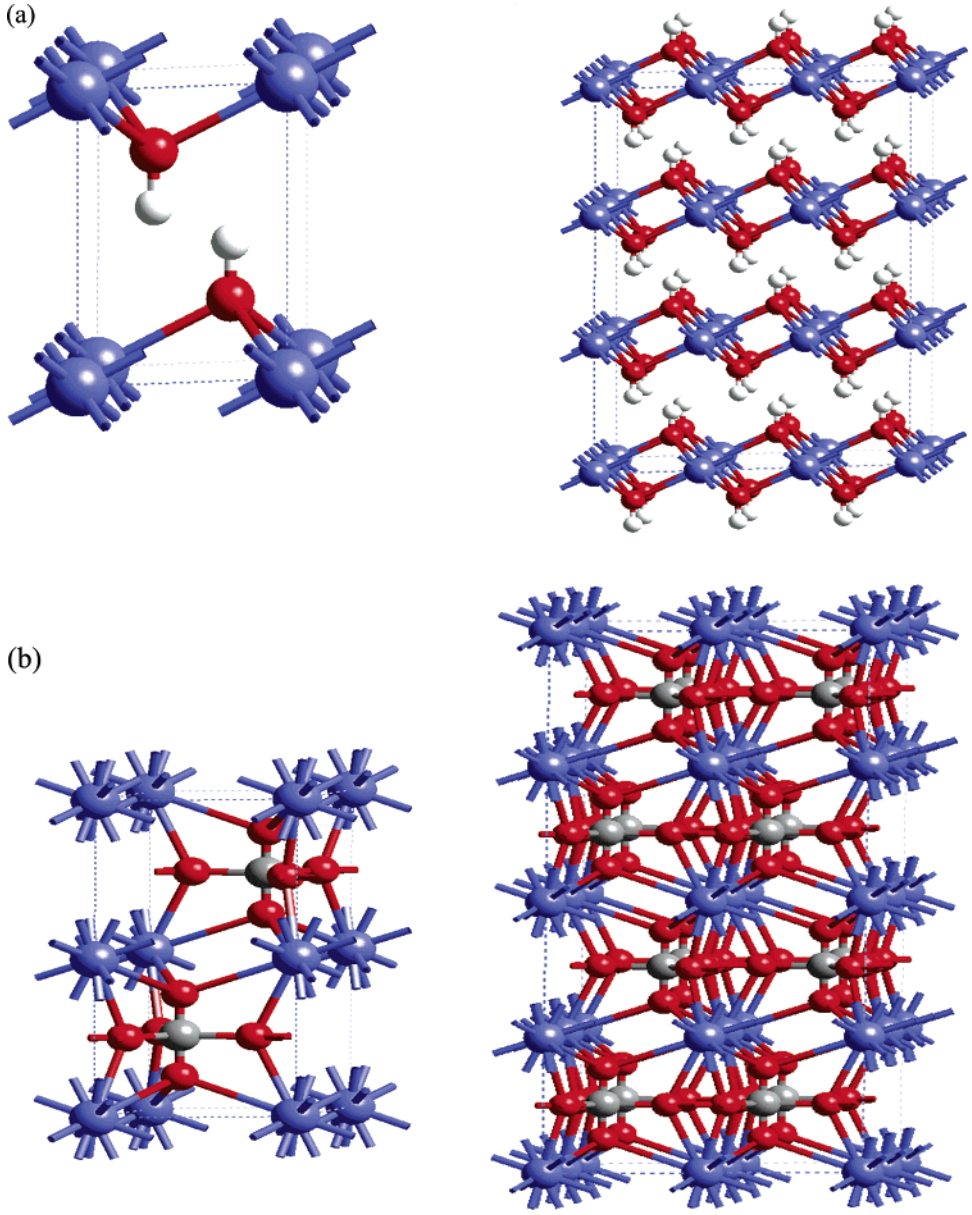

Figure 10. Unit cells of (a) portlandite (supercell 3 × 2 × 3) and (b) vaterite (supercell 2 × 2 × 2). Calcium in blue, oxygen in red, carbon in gray, and hydrogen in white.

one Oh). Figure 4b shows the packing arrangement of these different molecules in the unit cell.

The remaining compounds were also found to be monomeric by binding either three (**4a** and **5**) or four (**2**, **4a**, and **7**) THF molecules, where the number of solvent molecules decreases with increasing steric bulk of the ligand. The angles are consistent with slightly distorted Oh (**2**, **4a**, **7**; Figures 2, 4a, and 7, respectively) or TBP (**4a**, **5**; Figures 4a and 5, respectively**)** geometries. Literature monomeric $Ca(OR)_2$ compounds have reported Ca−O bond distances ranging from 2.32 to 2.42 Å[16,21] which are in agreement for **2** (av 2.33 Å), **4a** (2.32 Å), and **5** (2.32 Å). Compound **7** displays a Ca−O distance of av 2.34 Å that is substantially longer than that of the only other calcium siloxide derivative reported in the literature: 2.18 Å for $[(NH_3)_2(TPS)Ca(\mu\text{-}TPS)_3Ca(NH_3)_2]$.[37] Again, the limited data sets and different bound solvents make meaningful comparisons difficult.

Solution Behavior. To garner control over the final nanomaterials, it is necessary to understand the structure of the precursor and to determine if the solid-state structure was retained in solution. The dried crystals were, therefore, dissolved in their parent solvent, and spectra were obtained at room temperature. If the structures of **1** and **3** are retained in solution, one μ-OAr and one terminal OAr set of resonances should be noted. From the ^{1}H NMR data, only one set of broad OAr resonances was noted for both samples yielding only limited information. The ^{13}C NMR data also yielded one set of broad resonances and did lend some insights into the solution structure as discussed below.

For **3**, there was a single methyl resonance for the symmetric DMP ligand with several small shoulders also present. On the other hand, for **1**, the less symmetrical oPP ligated species, two types of alkyl groups were observed which indicates two types of OAr ligands are present in solution. From the spectra of **1** and **3** coupled with μ-O ligands, it is difficult to envision the disruption of these structures.[4,11,12,15,36] Instead, the ligands are most likely in dynamic exchange that is often noted for metal alkoxides

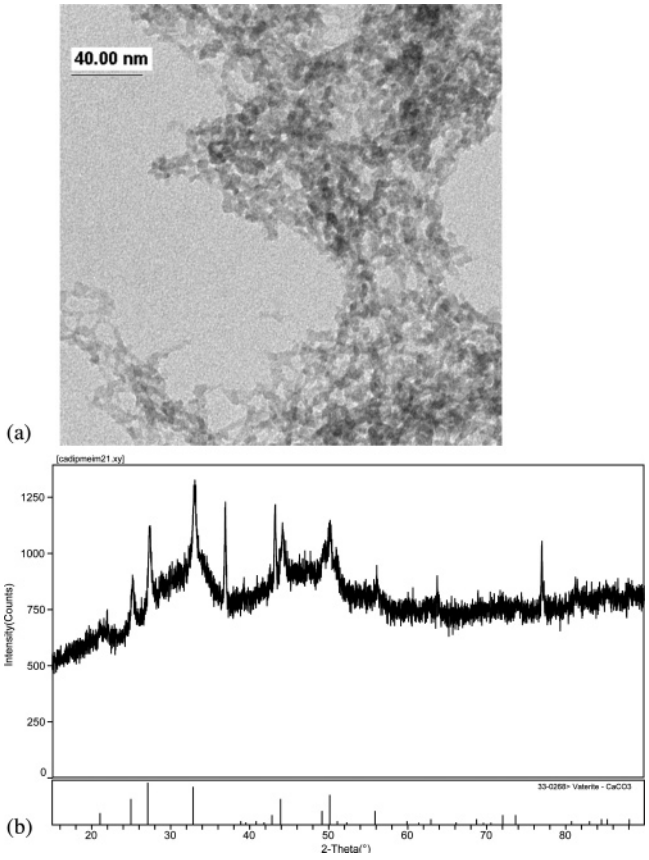

Figure 11. Characterization of vaterite nanomaterials formed from **4a** through the solution precipitation route: (a) TEM bright field image and (b) powder XRD pattern.

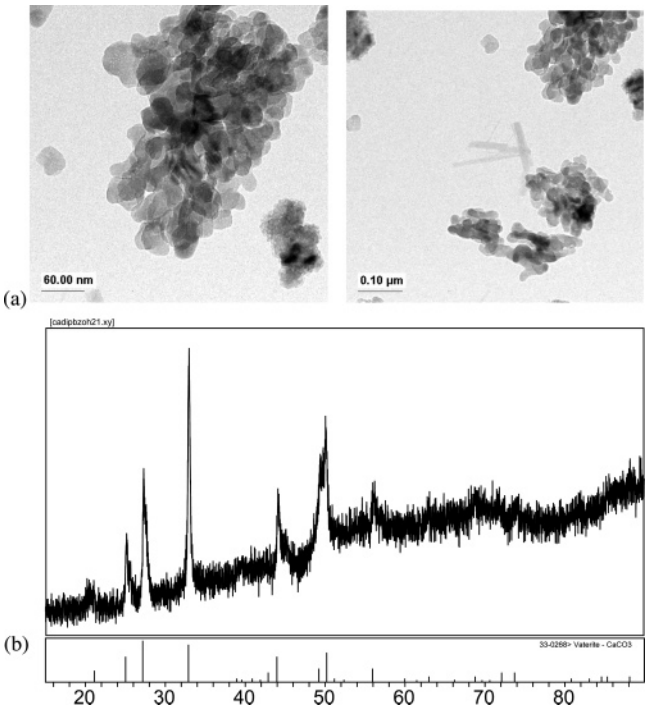

Figure 12. Characterization of vaterite nanomaterials formed from **4a** through the solvothermal route: (a) TEM bright field images and (b) powder XRD pattern.

upon dissolution.[4,11,12,15,36] The lower solubility of these compounds at slightly reduced temperatures prevented variable temperature NMR studies; therefore, it was reasoned that the tetranuclear complexes are maintained in solution with rapid exchange of the ligands producing the observed broad NMR spectra.

The monomeric solvated species noted for **2**, **5**, and **7** revealed only a single set of resonances, which is consistent with retention of the monomeric solvated species. Because each compound is redissolved in the parent solvent, the degree of solvation is most likely maximized. Therefore, for **4a**, it is unlikely that the two solvated species noted in the solid state are retained but solvated monomers such as "Ca(DIP)$_2$(THF)$_x$" as noted for **5** most likely form. The unsolvated dinculear species **6** displays only one set of resonances in tol-d_8 indicating that this species is disrupted, forming an unsolvated monomer. The steric bulk of the DBP ligand is well-known to stabilize unsolvated monomers.[16]

Materials Production. The hexanuclear **3** and mononuclear **4a** were selected for nanoparticle studies on the basis of their availability, solubility, and representation of the two major structural types observed for this family of compounds. Figures 8 and 9 show the characterization of the calcium ceramic nanomaterials generated using **3** following the solution precipitation or solvothermal route, respectively. For the solution route, the TEM images showed two types of particles: (i) rods approaching 10 × 60 nm in dimension and (ii) agglomerations of very small particles forming large particles on the order of 40−80 nm (Figure 8a). Attempts to obtain high-resolution TEM lattice images were unsuccessful because of rapid damage of the samples under the beam. The powder XRD pattern obtained (Figure 8b) on the bulk powder revealed that these particles were consistent with portlandite [or Ca(OH)$_2$] which is a member of the trigonal−hexagonal scalenohedral class (32/*m*) crystal system as shown in Figure 10.[44] Scalenohedral refers to a crystal whose faces are triangles with three sides that are unequal in length (scalene). Portlandite is the hydrolyzed product of Portland cement, hence the name, and one step removed from $CaCO_3$.[45]

The solvothermal route yielded rods of similar dimensions that appeared in a flower-like arrangement (Figure 9a). However, these structures also suffered damage under the electron beam, and the STEM bright field images revealed that the floral arrangement was really made up of unconnected rods, most likely formed because of a drying phenomenon. The powder XRD pattern (Figure 9b) of the bulk material indicated that this material was portlandite.[44] Three additional peaks were observed that were close to matching a series of (*h*00) peaks but did not index as portlandite. Because the TEM data did not reveal two phases, the powder XRD data were interpreted as a superlatice reflection in the *a* axis (four times to yield 14.3 Å). As a result of disorder of the *c* axis as evidence by broad peaks, this is not an unreasonable assumption.

It is interesting that both processing methods (solution and solvothermal) formed the hydroxide phase because the solvothermal route does not employ water as the decomposition agent and both routes yielded nanorods. The OH

(44) Desgranges, L.; Grebille, D.; Calvarin, G.; Chevrier, G.; Floquet, N.; Niepce, J. C. *Acta Crystallogr., Sect. B* **1993**, *49*, 812.
(45) Stepkowska, E. T.; Perez-Rodriguez, J. L.; Sayagues, M. J.; Martinez-Blanes, J. M. *J. Therm. Anal. Calorim.* **2003**, *73*, 247.

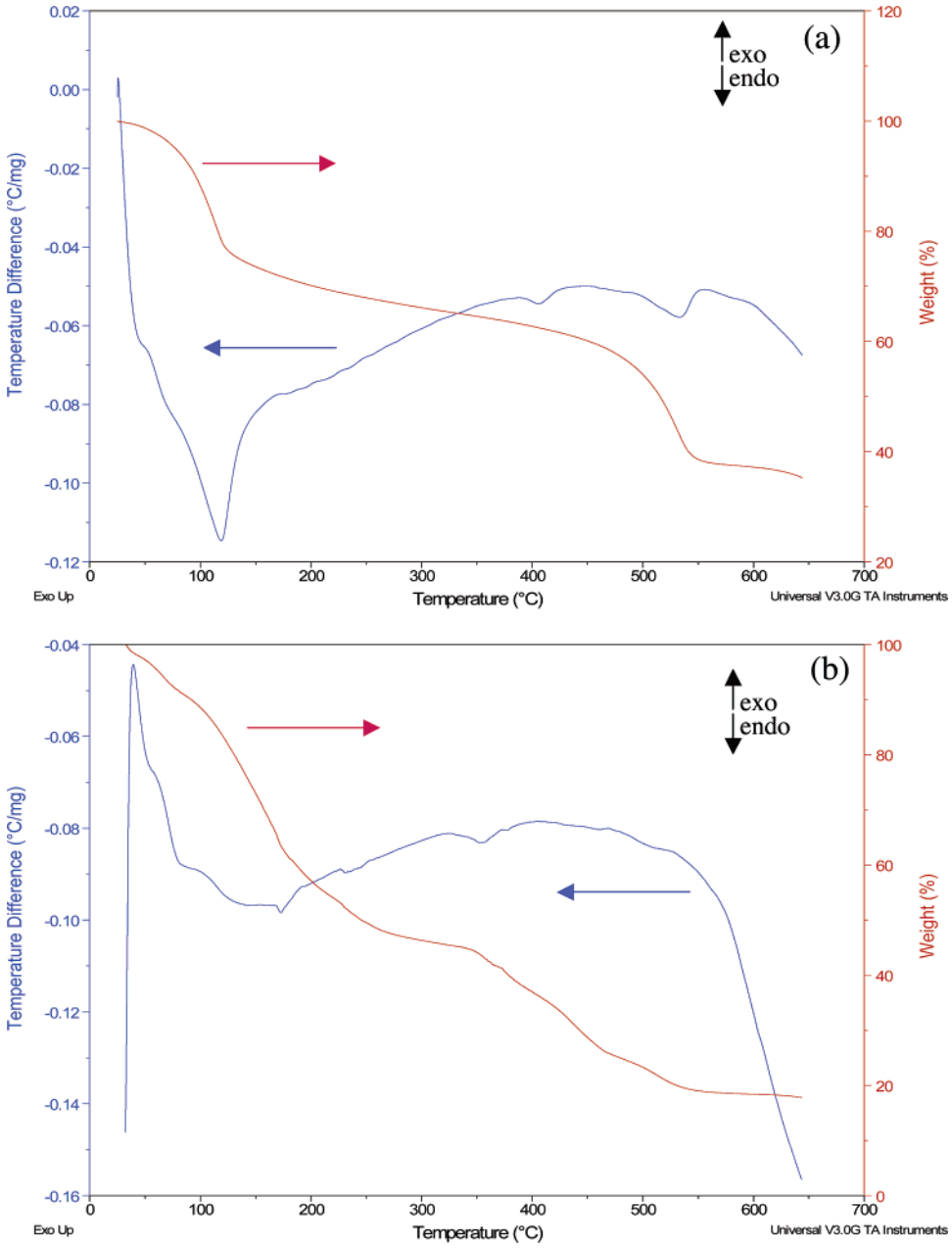

Figure 13. TGA/DTA spectrum of (a) **3** and (b) **4a**.

formation in the solvothermal route may result from the residual H noted in the X-ray structure of **3**. Additional work to understand the behavior of the alkoxides in benzyl alcohol is underway. If the PSA is used to explain the morphology of the final nanomaterials, then it is reasonable that rods were formed. If the organic moieties are removed from the structure of **3**, in general, the remaining Ca−O network resembles two face-shared cubes with opposite corners missing. Statistically, growth off of the sides of the shared cubes would be easier than on the ends because of the missing component. Hence, this preferred growth would generate particles that were significantly longer in one direction than the other, forming rods. This is similar to what was noted for the previously reported ZnO system.[4]

Figures 11 and 12 represent the nanomaterials generated using **4a** in the solution and solvothermal route, respectively. Compound **4** is a set of monomeric species and should make spherical particles based on the PSA. In agreement, the solution route generated small spherical particles on the order of 10−15 nm. In contrast, the solvothermal route yielded two morphologies: large particles (30−40 nm) and rods; however, the particles predominate. The few nanorods observed were on the order of 0.2 μm in length and ∼50 nm in width. Therefore, the PSA would apply to the CaO_x system as well, for the limited number of samples studied here.

We anticipated that the portlandite phase would be the favored phase for **4a**; however, the resulting nanomaterial was identified as vaterite ($CaCO_3$)[46] by powder XRD analysis for both processing routes. Vaterite is in the hexagonal−dihexagonal dipyramidal crystal system (see Figure 10) and is considered to be a meta-stable species, easily converting to calcite at low temperature or aragonite at elevated

(46) Meyer, H. J. *Z. Kristallogr., Kristallgeom., Kristallphys., Kristallchem.* **1969**, *128*, 183.

temperatures.[45,46] Only a handful of reports concerning the vaterite phase are available with most stabilized on a gold support.[47−50]

For this study, the resulting phase differences noted for **3** and **4a** can only be attributed to the precursors because the processing schemes were identical for both compounds. Therefore, it is important to understand why both **3** and **4a** form such drastically different phases, independent of the processing route. The PSA partially accounts for the morphological variations noted but does little to explain the observed phases.

Because compound **3** is partially condensed, it was assumed that this compound may undergo a different decomposition or PDP than that observed for the solvated alkoxide **4a**. Therefore, thermal decomposition of these materials under inert atmospheric conditions, up to 650 °C using TGA/DTA analyses, was explored. Figure 13 shows the TGA/DTA spectra for **3** and **4a**. For **3**, two weight losses are noted ending at ∼125 and 550 °C with a relatively stable weight loss between these temperatures. This implies that the ligands of **3** would be cleanly decomposed (i.e., ligand loss complete) under our experimental conditions. The stability after ligand loss would imply that a thermodynamic phase would be favored, resulting in the isolation of the portlandite phase.[45] In contrast, for **4a** numerous small weight steps were noted ending at ∼190, 350, 475, and 540 °C. This indicates that ongoing ligand decomposition occurs under our experimental conditions (200 °C). This continuous decomposition serendipitously allows the kinetically favored vaterite phase[45] to be "trapped" under the conditions explored in this experiment. Therefore, these two "$Ca(OR)_2$" precursors yield different morphologies based on PSA and different phases due to PDP variations.

Further work to verify the PDP as a means to control the phase was investigated through increased temperature at prolonged times. These processing changes would allow the particles to grow larger and change from the kinetic to the thermodynamic stable species. Powder XRD patterns of the resultant nanoparticles of **3** and **4a** from the solution route yielded portlandite for both routes. For **3**, this is not unexpected because the TGA/DTA data reveal a steady growth plane and the central core of the molecule most likely favors the thermodynamic stable portlandite. For **4a**, however, we have now moved away from the initial kinetic product, vaterite kinetic product toward a more stable thermodynamic product portlandite. The subsequent TEM images of **4a** revealed substantially larger particles lay the groundwork for the PDP as a means to control the phase of the final nanomaterials. Further work is needed to garner control over the PDP, but for the first time we have clearly demonstrated that the precursor plays a major role in the final phase isolated.

Summary and Conclusion

A new family of solvated calcium aryloxides derivatives were isolated (**1**−**7**). The majority of these compounds (**2**, **4a**, **5**, **7**) adopt a mononuclear arrangement as a result of solvation by THF; two complexes (**1** and **3**) form tetranuclear species using an oxo and aryloxide ligand set; compounds **6** and **4b** adopt dinculear structures. Solution NMR argues for retention of these structures in the parent solvent except for **6**, which appears to be disrupted into a monomer. When **3** and **4a** were used as representative solution species (tetra- and mononuclear), nanoparticles were generated following solvothermal and solution precipitation routes, the latter of which may be amenable to large scale preparation of calcium nanoceramic materials.

Morphological growth follows the PSA wherein the structure plays a large role in the final morphology. In this case, mononuclear species appear to form larger nanodisks or nanorods by the solvothermal route but smaller nanodots by the solution routes. Interestingly, the slightly different precursors yielded different phases, independent of how they were processed. The tetranuclear oxo species led to the thermodynamic favored portlandite phase while the mononuclear species yielded the kinetically stable vaterite. The idea of using PDP that is dictated by the precursor's structure to control the final phase of the resultant nanomaterial, independent of the processing methodology, is an overlooked aspect that should be considered when producing tailored nanomaterials.

Acknowledgment. The authors thank Ms. L.A. Ottley and Drs. R. T. Cygan and K. G. Ewsuk of SNL for helpful discussion as well as the Office of Basic Energy Sciences for support of this work. Sandia is a multiprogram laboratory operated by Sandia Corporation, a Lockheed Martin Company, for the United States Department of Energy under contract DE-AC04-94AL85000.

Supporting Information Available: CIF files for **1**−**7**. This material is available free of charge via the Internet at http://pubs.acs.org.

CM0700091

(47) Rautaray, D.; Kumar, P. S.; Wadgaonkar, P. P.; Sastry, M. *Chem. Mater.* **2004**, *16*, 988.
(48) Xu, Q.; Cai, W. Y.; Zhu, J. J. *Chem. Lett.* **2005**, *34*, 832.
(49) Andreassen, J. P. *J. Cryst. Growth* **2005**, *274*, 256.
(50) Andreassen, J. P.; Hounslow, M. J. *AIChE J.* **2004**, *50*, 2772.